Sputtering from ion-beam-roughened Cu surfaces

M. Stepanova and S. K. Dew
Department of Electrical and Computer Engineering, University of Alberta, Edmonton, Alberta, Canada T6G2V4

I. P. Soshnikov
Centre of Nanoheterostructure Physics, Ioffe Physico-Technical Institute, 26 Polytekhnicheskaya, St. Petersburg, 194021 Russia
(Received 26 February 2002; revised manuscript received 5 June 2002; published 24 September 2002)

A comprehensive theoretical and experimental study of sputtering from copper surfaces roughened by low-energy Ar^+ ion bombardment is reported. The total sputtering yields of thermally deposited Cu samples bombarded by 400-eV and 800-eV ions at 0°–70° angles of incidence have been measured and compared with a numerical model we have developed. To compute sputtering yields from rough surfaces, an original approach has been introduced, which accounts for sputtering anisotropy and shadowing of material emitted at grazing angles. The approach is flexible with respect to surface morphology and can be applied with any submicron structures. To specify the morphology that develops on the Cu surface under low-energy ion bombardment, the surface of bombarded Cu samples has been investigated by scanning electron microscopy. The morphology has been found highly unstable, appearing with random roughening, inclined conelike structures, ripples, or almost flat surfaces, depending on the bombardment conditions. For the samples considered it is found that the angular dependency of the total sputtering yield is strongly affected by surface morphology, which varies with the angle of ion incidence and bombardment energy. Approximations for accounting for the surface roughness required to describe sputtering at particular energy and angular regimes are discussed.

DOI: 10.1103/PhysRevB.66.125407 PACS number(s): 79.20.Rf, 61.82.Bg

I. INTRODUCTION

It is commonly known that ion bombardment modifies the surface morphology by producing submicron-sized roughness or, contrarily, causing surface polishing. Ion-induced formation of conic structures, pyramids, and ripples has been the focus of experimental and theoretic research for decades.[1–3] Recent studies emphasize the nanostructuring outcome of the phenomenon.[4–10] As can be seen from available experiments, the surface morphology that develops due to the ion bombardment is strongly sensitive to the ion species, as well as energy and angle of incidence.[1–5,10] In particular, the angular dependence of ion-induced roughness is being actively addressed in the literature.[4,5,7] The surface morphology is found to be strongly related to the direction of the ion beam, and can present as conelike structures,[4] or as ripples aligned normal[7,8] or parallel[5,7] to the beam plane.

Ion-induced surface roughening has been qualitatively understood in the framework of the kinetic theory suggested by Bradley and Harper[11] and developed by Carter[12,13] and Barabási and co-workers.[14–17] The approach is based on the Sigmund theory of isotropic collision cascades,[18,19] after which the sputtering rate scales with the product of the local ion flux and the local deposited energy. This allows accounting for the surface curvature through an increase of the local sputter rate at troughs and a decrease at crests.[19,11] The resulting positive feedback enhances a surface's unevenness and leads to a self-maintained roughening. However, the traditional theory of isotropic sputtering disregards the cascade anisotropy, and therefore is confined to keV and higher bombardment regimes, when the isotropic approximation is justified. Also the theory is known to overestimate the sputtering rates at grazing local angles of incidence.[18] Consequently, in spite of the elegant accounting for the surface curvature, the kinetic theory of surface roughening is still rather qualitative.

We believe that the way towards a better understanding of ion-induced roughening lies through a more accurate accounting of sputtering yields from uneven surfaces. Furthermore, a comprehensive theoretical description and/or simulation of total and differential sputtering yields from realistic rough surfaces responds to the existent need in modeling of sputter particle sources for various deposition processes. However, understanding of sputtering from rough surfaces is far from complete. Major analytic results have been obtained without accounting for sputtering anisotropy and overlooking shadowing of particles emitted at grazing angles.[13,15,16] Some binary-collision simulations of sputtering from rough surfaces[20,21] do address a few particular target morphologies with fractal topography[20] and random roughness,[21] but do not consider other frequently encountered structures, such as cones or ripples. As far as experiments are concerned, studies with both measurements of the sputtering yield together with a complementary survey of the surface morphology are extremely rare. Particularly, surface roughness that develops at the sub-keV bombardment regime, which is relevant for many nanofabrication techniques, appears to be overlooked by experiments.

In this paper we present a comprehensive theoretical and experimental investigation of sputtering from copper surfaces roughened by sub-keV ion bombardment. In Sec. II, an original approach is introduced to compute sputtering yields from rough surfaces, which accounts for sputtering anisotropy and shadowing. The approach is flexible with respect to surface morphology and can be applied with any submicron structures. To specify the morphology that develops on a Cu surface under low-energy ion bombardment, the surface of Ar^+ bombarded Cu samples has been investigated by scan-

 ©2002 The American Physical Society

ning electron microscopy (SEM) at various angles of incidence. The total sputtering yields also have been measured. We outline the experimental techniques employed in Sec. III. The effect of ion-induced surface morphology on the total sputtering yield is investigated in Sec. IV by comparison of our experimental results with theoretical modeling. Conclusions are summarized in Sec. V.

II. THEORY

We consider sputtering of an uneven surface parallel to the $\{x,y\}$ plane of the laboratory frame, with the axis z directed inward with the surface's overall normal. The incoming ionic beam lies in the $\{x,z\}$ plane. The beam's direction is defined by the unit vector $\mathbf{n}_i=\{\theta^i,0\}$, θ^i being the angle of incidence with respect to the laboratory-frame axis z. Because the surface is rough, its local areas have various orientations defined by the local inward normal $\mathbf{n}_s=\{\theta_s,\varphi_s\}$, where θ_s and φ_s are laboratory-frame polar and azimuthal angles, respectively. We describe the surface with the distribution of local orientations $\omega(\mathbf{n}_s)$, which is normalized, as

$$\int \omega(\mathbf{n}_s)d\mathbf{n}_s=S/S_0, \tag{1}$$

where S is the area of the rough surface and S_0 is the corresponding flat area in the plane $\{x,y\}$. For each surface orientation, $\mathbf{n}_s$, the ionic beam makes the local angle of incidence θ^i_{loc} with respect to $\mathbf{n}_s$. Sputtering of particles from the local surface element $d\mathbf{n}_s$ is described as for the flat surface for the angle of incidence θ^i_{loc}. This gives the local differential sputtering yield $Y(\theta^i_{\mathrm{loc}},\mathbf{n}_{\mathrm{loc}})$, with $\mathbf{n}_{\mathrm{loc}}=\{\theta_{\mathrm{loc}},\varphi_{\mathrm{loc}}\}$ the direction of emission with respect to the reference frame related to the local direction $\mathbf{n}_s$. Respective laboratory-frame distribution of sputtered particles, $Y(\mathbf{n}_s,\mathbf{n})$, is given by

$$Y(\mathbf{n},\mathbf{n}_s)d\mathbf{n}=Y(\theta^i_{\mathrm{loc}},\mathbf{n}_{\mathrm{loc}})d\mathbf{n}_{\mathrm{loc}}, \quad \cos\theta^i_{\mathrm{loc}}=\mathbf{n}_i\cdot\mathbf{n}_s,$$

$$\mathbf{n}=T_s\mathbf{n}_{\mathrm{loc}}, \tag{2}$$

the symbol T_s denoting the coordinate transformation from the local to the laboratory reference frame.

Some particles that have been sputtered are redeposited[21] and do not contribute to the total sputtering yield. We account for this shadowing effect through the coefficient $P(\mathbf{n},\mathbf{n}_s)$, which represents the probability for a particle emitted from the local surface element $\mathbf{n}_s$ in the direction $\mathbf{n}$ to avoid being redeposited. The total sputtering yield from a rough surface is thus given by the integration

$$Y=(\cos\theta^i)^{-1}\int \omega(\mathbf{n}_s)\int \cos\theta^i_{\mathrm{loc}}Y(\mathbf{n},\mathbf{n}_s)$$

$$\times P(\mathbf{n},\mathbf{n}_s)d\mathbf{n}d\mathbf{n}_s, \quad \cos\theta^i_{\mathrm{loc}}>0. \tag{3}$$

The computation is done in two steps. First, we compute the differential sputtering yield for a flat surface $Y(\theta^i_{\mathrm{loc}},\mathbf{n}_{\mathrm{loc}})$, as a function of the angle of incidence θ^i_{loc}. For this purpose we solve numerically a set of master equations, as discussed in detail in Ref. 22. In contrast to traditional analytic theories, our approach accounts for the deflection of incoming ions and emitted particles when they pass the surface at oblique angles,[22] which provides more realistic angular dependencies for the total and differential sputtering yields. The theory[22] is adapted specifically for sub-keV sputtering regimes.

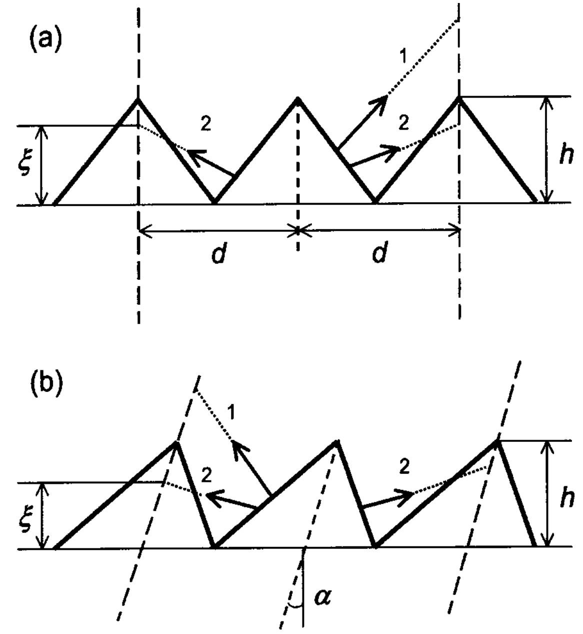

FIG. 1. Sketch of the surface structures considered. (a) represents a cross section for straight cones and triangular ridges, and (b) the one for inclined cones. The arrows indicate the directions of emitted particles, and the long-dashed lines show the cross section of the imaginary shadowing wall. The particles labeled "1" are sputtered, whereas those labeled "2" are shadowed partly (for cones) or totally (for ridges).

At the second stage of the computation, the laboratory-frame differential yields $Y(\mathbf{n},\mathbf{n}_s)$ are obtained from Eq. (2) and inserted in Eq. (3). The distribution $\omega(\mathbf{n}_s)$ and the probability $P(\mathbf{n},\mathbf{n}_s)$ are defined individually for each surface morphology. We have considered three kinds of structures: straight cones [Fig. 1(a)], inclined cones [Fig. 1(b)], and triangular ridges [again, Fig. 1(a)]. We describe the surface structure with the parameter $\eta=h/d$, h being the height of the structures and d being the distance that separates neighboring structures. For inclined cones, which have an elliptic base, d is the ellipse's smaller axis. Inclined cones are also described with the angle α between the cone's axis and the surface normal, as shown in Fig. 1(b). Our approach allows any orientation of the inclined cones and ridges with respect to the ionic beam, so we do not specify their orientation at this point.

Finally, shadowing must be taken into account. We select a representative structure (a cone or a ridge) and consider emission from a point $\{x_s,y_s,z_s\}$ on its surface. For the structures considered, z_s is the height with respect to the cone's or ridge's base and $\{x_s,y_s\}$ define the local surface orientation $\mathbf{n}_s$ with respect to the laboratory frame. Thus, for a selected structure, any source location can be described with the coordinates $\{\mathbf{n}_s,z_s\}$. Next, we describe local direc-

tions of emission by vectors $\mathbf{n}_{loc}=\{\theta_{loc},\varphi_{loc}\}$. The local polar emission angles θ_{loc} range between 0 and $-\pi/2$, and local azimuth emission angles φ_{loc} range between 0 and 2π with respect to a local reference frame related to $\mathbf{n}_s$. For each local emission direction $\mathbf{n}_{loc}$, we obtain the respective laboratory-frame emission direction $\mathbf{n}=T_s\mathbf{n}_{loc}$, and determine the probability to avoid the redeposition P as a function of the source location $\{\mathbf{n}_s,z_s\}$.

It is convenient to subdivide the shadowing mechanisms into two categories. First, some emission directions have a positive z projection $\mathbf{n}\cdot\mathbf{z}>0$, which means that particles move towards the surface and therefore cannot be sputtered. Thus, our first shadowing condition is

$$P(\mathbf{n})=0, \quad \mathbf{n}\cdot\mathbf{z}>0. \tag{4}$$

For the structures considered, the condition (4) does not depend on the source location $\{\mathbf{n}_s,z_s\}$ after $\mathbf{n}$ is defined.

The particles that have $\mathbf{n}\cdot\mathbf{z}<0$ move away from the surface and potentially can be sputtered. However, obliquely emitted particles can be redeposited on neighboring structures, as sketched in Fig. 1. We account for this shadowing mechanism by considering the passage of sputtered particles through an imaginary wall around the surface structure. The cross section of the wall is shown in Fig. 1 by long-dashed lines. For straight cones, the wall is a cone-centered cylinder with the radius d. For inclined cones, the wall is a similarly inclined elliptic cylinder with the size of the base equal to double the size of the cone's base. For the ridges, the wall consists of two vertical planes parallel to the ridge. We consider the height of intersection with the wall ξ for each direction of emission. When $\xi>h$, as for the directions "1" in Fig. 1, the probability of passage P is equal to unity. Otherwise, as in the cases labeled "2" in the figure, the probability P is assumed equal to ξ/h for cones and zero for ridges. The height ξ is the function of the laboratory-frame emission direction $\mathbf{n}$ and on the source location $\{\mathbf{n}_s,z_s\}$, and so is the respective probability of the passage. Therefore, our second shadowing condition reads

$$P(\mathbf{n},\mathbf{n}_s,z_s)=\begin{cases}\zeta(\mathbf{n},\mathbf{n}_s,z_s)/h & \text{cones,}\\ 0 & \text{ridges,}\end{cases} \quad 0\leqslant\zeta(\mathbf{n},\mathbf{n}_s,z_s)\leqslant h. \tag{5}$$

To obtain z_s-independent probability of passage, we take the average,

$$P(\mathbf{n},\mathbf{n}_s)=\int_0^h w(\mathbf{n}_s,z_s)P(\mathbf{n},\mathbf{n}_s,z_s)dz_s. \tag{6}$$

In Eq. (6), the weighting function $w(\mathbf{n}_s,z_s)$ is normalized so that $\int_0^h w(\mathbf{n}_s,z_s)dz_s=1$. This function describes the relative contributions from local sources with the same orientation $\mathbf{n}_s$, but different heights z_s. For example, ridges have just $w=1/h$, whereas for straight cones $w(z_s)=2(h-z_s)/h^2$. For inclined cones, w is a function of both $\mathbf{n}_s$ and z_s.

To our knowledge, similar approaches reported by other authors disregard the effect of shadowing,[13,15,16] or account for it in a simplistic way through a universal probability $P(\theta)$ that depends only on the laboratory-frame polar angle of emission θ.[21] Also our angle-resolved local sputtering rate accounts for the sputtering anisotropy, which makes the approach applicable for sub-keV bombardment and provides a more realistic function of the local angle of incidence θ^i_{loc}.[22] However, we do not consider the surface curvature since this paper concentrates on the sputtering yields rather than on a self-consistent modeling of surface roughening. Potentially, the influence of the curvature can be introduced in Eq. (3) through an additional integration over the rough surface with an appropriate weighting function, but it would give only a minor correction to the total yield.

Our approach is applicable with any surface morphology, unless the surface structures are too tiny to apply the flat-surface approximation for local angular distributions. For the ion energy regimes considered, the theory presented is expected to describe sputtering of submicron-sized structures with an acceptable accuracy. Note also that our approach can be easy generalized to provide angular and angle-resolved energy distributions of sputtered particles, although we do not consider the differential yields in this paper.

III. EXPERIMENT

Copper samples for our sputtering studies have been prepared by physical vapor deposition using a VUP-5 SELMI (Ref. 23) thermal evaporation unit (base pressure less than $1-2\times10^{-6}$ Torr). Industrial 99.98% pure copper sources were employed. For substrates, monocrystalline (001) boron-doped, 7.5-Ω cm silicon wafers were used. The deposition provided 500–1000-nm-thick Cu films. Tests by x-ray diffraction do not reveal much texture in the films prepared this way. The state of the surface of the samples used in this work has been characterized by scanning electron microscopy (SEM) with the CamScan 4-88 facility. As-deposited surfaces have been investigated by SEM. The surfaces had random ~1–4-nm-sized roughness.

The deposited Cu samples have been subsequently bombarded by 400- and 800-eV Ar beams at room temperature. Before bombardment, the samples were partly masked in order to obtain well-defined steps from the sputter erosion. A specially designed duoplasmatron ion gun[24] provided a 50-mm-wide, well-collimated, 95% neutralized Ar beam with the flux density of 0.7×10^{15} and 1.3×10^{15} $\text{cm}^{-2}\,\text{s}^{-1}$ for 400- and 800-eV energies, respectively. The determination of the ion flux has been performed by sputtering reference GaAs samples for which the sputtering yields have been previously tabulated.[25] The sample holder allowed positioning the samples at angles of 0°–75° between the surface normal and the bombarding beam. The 400-eV bombardment was for 15-min duration, and that of the 800-eV bombardment was for 10 min. This made 100–300-nm-deep sputter craters, depending on the angle of ion incidence. The sputtering yields were determined by measurement of the height of the step after removal of the mask. A DEKTAK-3030 profilometer was used for these measurements. The surface morphology of the Cu samples after the bombardment was investigated by SEM.

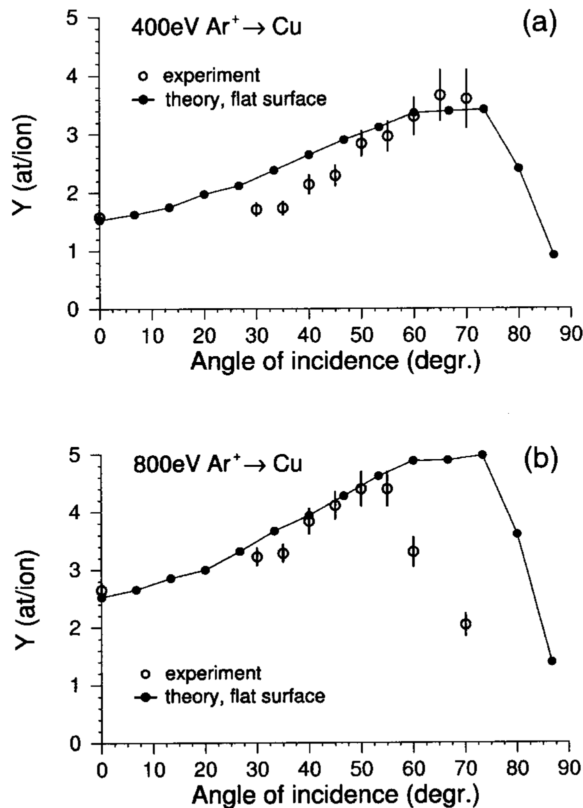

FIG. 2. Dependence of the total sputtering yield on the angle of ion incidence with respect to the laboratory-frame surface normal for 400- (a) and 800-eV (b) bombardment energies, as measured and computed for a flat surface.

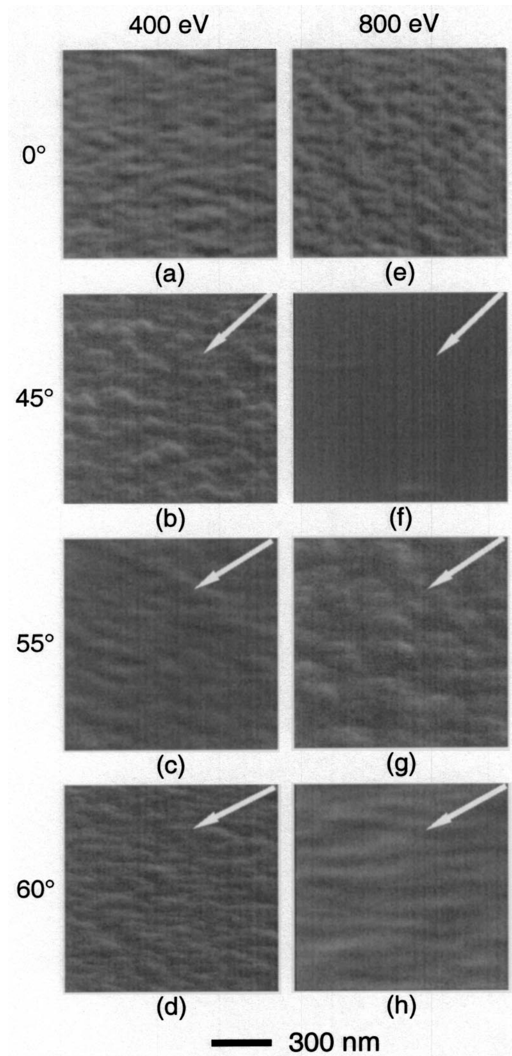

FIG. 3. SEM microphotographs of Cu surfaces bombarded by 400- and 800-eV ions at 0°, 45°, 55°, and 60° incidence. The arrows indicate the direction of the ion beam. The angle between the surface normal and the image's plane was 27° (a)–(e) and 12° (f)–(h).

IV. DISCUSSION

A. Experimental results

Figure 2 presents the measured total sputtering yields for Cu bombarded by 400- and 800-eV ions at varying angles of incidence with respect to the surface normal, compared to our numerical results for a flat surface.[22] For 400-eV bombardment, the agreement is reasonable for normal incidence and at grazing angles $\theta^i > 50°$. However, at the angles $\theta^i = 30° - 45°$ the measured yield is very close to that at normal incidence, whereas the computation predicts a steady increase of the yield until $\theta^i \approx 75°$. For 800-eV bombardment, the computation overestimates the yield significantly at the angles θ^i surpassing 50°, and the maximum of the computed dependence is shifted by 20° towards larger angles with respect to the experiment.

It has been already demonstrated that surface roughness decreases the sputtering yield at oblique ion incidence,[21] so that it is natural to expect the difference to result from surface morphology. We therefore have investigated the state of the surface of bombarded copper samples by SEM. The microphotographs obtained for 0°, 45°, 55°, and 60° incidence are presented in Figs. 3(a)–(h). As can be seen, 400-eV bombardment at normal and 45° incidence produces submicron-scaled random roughness. At 55° incidence, the surface structures become smoother, but the roughness recovers at $\theta^i = 60°$. For 800-eV ion energy, normally incident bombardment also generates a random morphology. However, 45° incidence does not produce a significant roughness, at least at the submicron scale. At $\theta^i = 55°$, the roughness reappears with conelike structures inclined toward the direction of the beam. Finally, a rippled structure aligned parallel to the projection of the beam on the surface arises at $\theta^i = 60°$. Thus, at least four different kinds of morphology can be identified on the Cu surface:

(i) random roughness, Figs. 3(a), 3(b) and 3(e);
(ii) even surface, Fig. 3(f);
(iii) structure inclined preferentially towards the beam, Fig. 3(g); and
(iv) ripplelike structure aligned parallel to the beam plane, Fig. 3(h).

We restrain ourselves from definitive conclusions in respect to Figs. 3(c) and 3(d), but suppose the morphology in Fig. 3(c) to be a transitory one between the (iii) and (iv) regimes, and that in Fig. 3(d) to fall into the (iii) category.

Comparison of 400-eV and 800-eV bombarded surfaces reveals important similarities. For both 400 and 800-eV beam energies, the surface morphology is highly unstable in the angular regime of 45°–60°; furthermore, in both cases the morphological transformations include surface smoothening [Figs. 3(c) and 3(f)] followed by a recovering of surface roughness with likely related morphologies [Figs. 3(d) and 3(g)]. The difference between 400 and 800 eV is, first, that the morphological transformations are better pronounced at higher ion energy: smoothening comes down to a fairly flat surface in Fig. 3(f) versus a partial blunting in Fig. 3(c), and inclined structures are better pronounced in Fig. 3(g) than in Figs. 3(c) or 3(d). Also pronounced ripples have not been detected with 400-eV bombardment in the angular regimes considered.

The observed morphological instability between approximately 45° and 60° angles of incidence corresponds well to the kinetic theory,[11,12,14] which predicts phase instability of ion-bombarded surfaces roughly in the same angular regimes. Also the theory[11,12,14] predicts formation of ripples parallel to the beam plane at grazing incidence, as detected in Fig. 3(h). However, the morphological phase diagrams given in Refs. 12 and 14 forecast a shift of the phase transformations towards larger angles of incidence with the increase of ion energy. Our experiment does not seem to confirm this prediction, demonstrating rather an opposite trend. This mismatch can be rationalized by supposing that sputtering by low-energy ions cannot be described in the same terms of average spatial distributions of deposited energy, as adopted in Refs. 12 and 14 for keV regimes.

Indeed, the low-energy bombardment does require a more detailed description of the energy deposition and sputtering. In the next section, we concentrate on total sputtering yields from the Cu surfaces roughened by low-energy bombardment, taking as a basis our recent model of anisotropic sub-keV sputtering.[22]

B. Modeling

We have investigated sputtering of the rough surfaces numerically. We approximate the random structures shown in Figs. 3(a), 3(b), and 3(e) with straight cones, as sketched in Fig. 1(a). The morphology seen in Figs. 3(g) and, presumably, 3(d) is approximated with inclined cones [Fig. 1(b)]. From the symmetry considerations, one could expect the cone's axis to be parallel to the ion beam, $\alpha=\theta^i$. However, Fig. 3(g) suggests a deviation from the beam direction, so

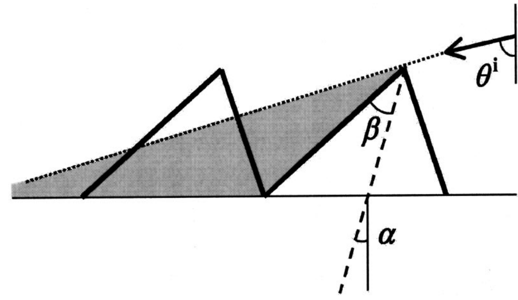

FIG. 4. Shadowing of the ionic beam at grazing incidence. The arrow indicates the direction of the beam, and the angles α and β define the direction of the cone's axis and the top half-angle.

that $\alpha<\theta^i$. We assume, rather arbitrarily, the empirical relation $\alpha=\theta^i/2$, expecting it to provide acceptable qualitative trends. Finally, we try triangular ridges directed parallel to the projection of the ion beam on the surface to approximate the morphology shown in Fig. 3(h). The three first lines in Table I list the above structures. In the following we denote the structures, as indicated in the last column in the table.

The structures considered have limitations with respect to the angles of ion incidence. At grazing incidence, shadowing of the ion beam occurs with straight and inclined cones, as illustrated in Fig. 4. Because the shadowed areas are not sputtered, such structures cannot be stable and therefore are not considered. The ripples parallel to the beam plane, which are approximated with the ridges, also have geometric limitations,[11–14,17] although these are not so straightforward. Based on our and published[4,5,7] experiments and on the theory,[11–14,17] we consider the ridge geometry for $\theta^i>50°$. The adopted conditions are summarized in the third column of Table I.

Figure 5 presents dependencies of the sputtering yield on the roughness parameter η, calculated for 0°, 30°, and 60° incidence with various surface structures. The results for 400- and 800-eV bombardment show similar trends, so that

TABLE I. The structures considered in this work. The meanings of the angles α, β, and ψ appear from Figs. 4 and 7(c), respectively.

Structure	Direction	Angular regimes considered	Label
Straight cones	$\alpha=0$	$\theta^i<\beta$	CS
Inclined cones	$\alpha=\theta^i/2$	$\theta^i<\alpha+\beta$	CI
Ridges	aligned parallel to the beam plane	$\theta^i>50°$	R
Pyramids	$\psi=5°-15°$	$\theta^i>50°$	P

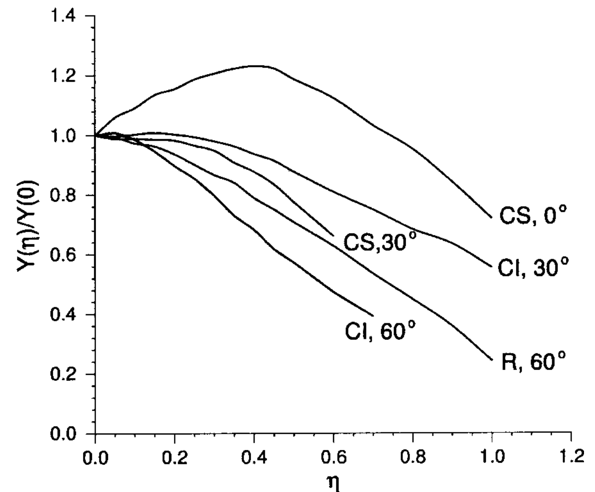

FIG. 5. Dependence of the normalized yield on the roughness parameter η, computed with various structures for 0°, 30°, and 60° incidence. The labels employed for the structures are listed in Table I.

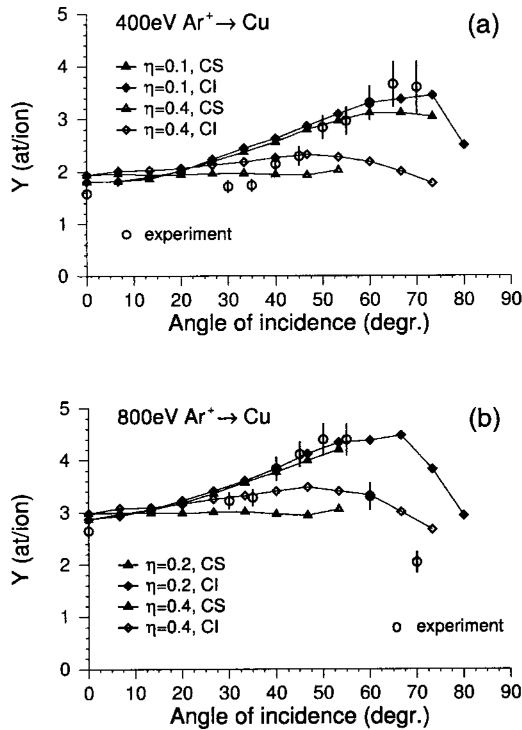

FIG. 6. Angular dependencies of the total yield computed for 400- (a) and 800-eV (b) bombardment with CS and CI structures for selected η roughness values, compared to the experimental results.

the presented dependencies for 800 eV are representative of both cases. As can be seen, at normal incidence the yield increases slightly with increasing roughness up to $\eta \approx 0.4$ where it reaches the maximum, although at oblique incidence the yield stays nearly constant until $\eta \approx 0.1$-0.2, and thereafter decreases for all geometries considered. This behavior differs significantly from that reported by Makeev and Barabási[15,16] and Carter,[13] who found a considerable increase of the yield with a comparable parameter for normally aligned sinusoidal ripples[15,13] and random roughness[16] at oblique incidence up to $\eta = 0.3-0.4$. We attribute lower sputtering yields obtained in this work to our accounting for the sputtering anisotropy together with the inclusion of shadowing. In our model, shadowing cuts out a considerable part of atoms emitted in forward local directions, where the emission is enhanced due to the cascade anisotropy.[22]

Figure 6 demonstrates the angular dependencies of the total yield computed with two kinds of cones for selected η values, in comparison with the experimental results. Unfortunately, the surface roughness (η) varies with angle which complicates interpreting the results. It can be seen that accounting for the roughness softens the angular dependency of the total yield. At η values greater than approximately 0.35, the calculated sputtering yield becomes almost insensitive to the angle of ion incidence. We believe that this explains why the sputtering yields measured at $\theta^i = 30° - 45°$ for 400-eV bombardment are close to the normally incident case. As seen in the figures, the results with $\eta = 0.4$ agree closely with the experiment in those angular regimes for both ion energies. At the same time, significantly smaller η parameters are required when θ^i surpasses 40°–45°, reaching the regimes of morphological instability. At $\theta^i = 50° - 70°$ for 400-eV bombardment and $\theta^i = 40° - 55°$ for 800-eV bombardment, the experimental results are well described assuming a flat surface (Fig. 2) or cones with $\eta \leqslant 0.2$, in accord with the smoothening of the surface detected in Figs. 3(c) and 3(f). However, Figs. 3(d) and 3(h), which also correspond to the angular regimes in question, show a developed roughness. Respective experimental parameters η_{exp} can be estimated as approximately 0.2–0.3, which is larger compared to the fit theoretic values $\eta \leqslant 0.2$. We explain the difference by the fact that the observed inclined structures have softer tops in comparison to cones, which leads to softer slopes. Thus, cones with smaller η values would provide a better approximation.

Under 800-eV bombardment, the surface morphology changes to a rippled structure at 60° incidence [Fig. 3(h)], and the sputtering yield falls off abruptly at the same angle. In Fig. 7(a) we compare the grazing-angle portion of the

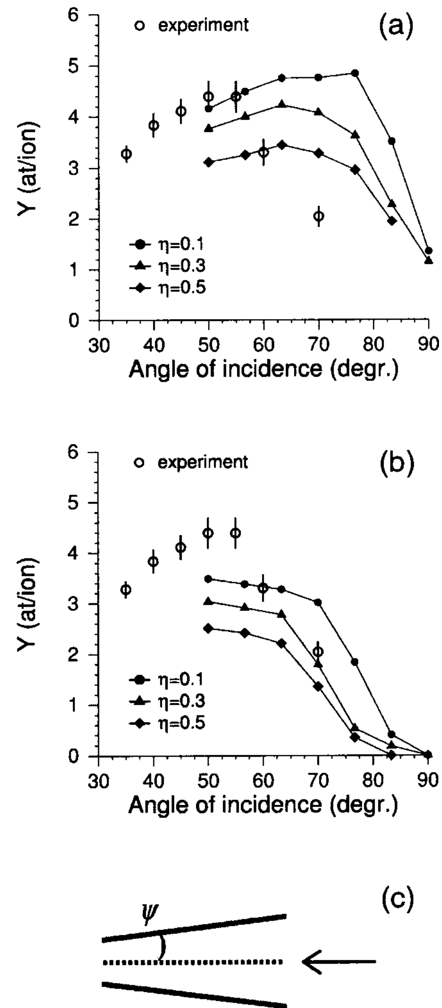

FIG. 7. Grazing-angle portion of the angular dependence of the sputtering yield computed for 800-eV bombardment with ridges (a) and elongated pyramids (b) compared to the experimental results. Sketch of the pyramid structure (c) shows the intersections of the sides with the (x,y) plane (solid lines), and the pyramid's ridge (points), which follows the projection of the ion beam on the surface (arrow).

TABLE II. Selected approximations to model sputtering at various angles of incidence for 400- and 800-eV bombardment of Cu by Ar^+.

	Ion energy (eV)		
	400		800
Incidence angles	Approximations	Incidence angles	Approximations
0°	CS, $\eta=0-0.2$	0°	CS, $\eta=0-0.2$
30°–35°	CI, $\eta=0.4-0.5$	30°–35°	CS, CI, $\eta=0.2-0.4$
40°–45°	CS, $\eta=0.2-0.3$; CI, $\eta=0.3-0.4$	40°–55°	CS, CI, $\eta=0-0.2$
50°–70°	CS, CI; $\eta=0-0.1$	60°–70°	P, $\eta=0.3-0.4$

experimental angular dependencies with our numerical results for the ridges aligned parallel to the beam plane. An important conclusion is that the ridge geometry does not explain the observed decrease of the yield at $\theta^i \geqslant 60°$, at least with reasonable η values. We thus have considered other approximations for the morphology appearing in Fig. 3(h). Reasonable results have been obtained assuming elongated-pyramid structures with sides making a small (5°–15°) angle ψ with respect to the projection of the ionic beam on the surface, as sketched in Fig. 7(c) and listed in Table I. Because of the dominant contribution of sputtering from the pyramid's sides, the emission from its front side has not been considered. Due to larger local angles of incidence θ^i_{loc}, the pyramidal structure provides a smaller sputtering yield in comparison to regular ripples. The examples for $\psi=10°$ presented in Fig. 7(b) show that the angular dependencies of the sputtering yield computed with $\eta=0.3-0.4$ agree well with the experimental results for $\theta^i > 60°$.

It can be summarized that a number of various approximations are required to describe the ion-induced surface roughness of Cu, according to the surface morphology that develops at given bombardment conditions. Table II lists the approximations that provide acceptable sputtering yields for various angular regimes at 400-eV and 800-eV bombardment. The postulated values for η are consistent with the experimentally observed trends in surface roughness.

V. CONCLUSIONS

We have introduced an original approach to compute the sputtering yield from rough surfaces. The sputtering yield is provided by integration over local angle-resolved contributions, which allows accounting for sputtering anisotropy and shadowing of sputtered material. Also, the angular dependencies of the total and differential local yield are obtained from this more inclusive model,[22] which is adapted specifically for sub-keV ion bombardment. As a result, even a slight surface roughness has been found to decrease the total yield at oblique incidence, in contrast to the results published for higher-energy regimes.[13,15]

Our experimental results demonstrate that the angular dependencies of the total sputtering yield for thermally deposited copper samples after 400- and 800-eV bombardment are significantly affected by surface morphology. Comparison of our numerical and experimental results has revealed following trends:

(i) Only minor changes of the total sputtering yield relative to the normal-incidence case are found for the angles of incidence under 35°–40°. This insensitivity can be explained by well-developed random roughness in this angular regime. The total sputtering yield can be computed assuming straight or inclined cones with the roughness parameter $\eta=0.2-0.5$.

(ii) At the angles of incidence of 45°–55°, the state of the surface is found to be highly unstable. Although a number of various morphologies are observed in this angular regime, corresponding sputtering yields can be obtained under a unified approximation, assuming minor straight or inclined cones with the parameter $\eta \leqslant 0.2$.

(iii) Under 800-eV bombardment, ripples aligned parallel to the beam plane are found at 60° incidence, which is accompanied by a sharp decrease of the sputtering yield. To describe this behavior of the yield, a special pyramidal structure is suggested with sides making a 5°–15° angle with respect to the projection of the ionic beam on the surface.

Our results demonstrate that surface morphology varies with the angle of ion incidence and ion energy, so that particular energy and angular regimes require individual approximations to account for the surface roughness. In the framework of our model, appropriate surface structures have been found to describe the observed sputtering yields quantitatively with an acceptable accuracy.

Potentially, the introduced approach can provide a quantitative self-consistent theory of sputter roughening, to predict surface morphologies along with sputtering yields. However, to be included into self-consistent models of roughening, our approach must be upgraded by an accounting of the surface curvature. Since the existing curvature-accounting technique[19,11] has not been justified for the sub-keV regime, this point is a nontrivial one and warrants further investigation.

ACKNOWLEDGMENTS

The authors thank V. Barchenko for his helpful discussions and assistance with preparation of the copper samples, and V. Busova and S. Belova for their help with SEM characterization and profilometric measurements. M.S. and S.K.D. acknowledge the support by the Natural Sciences and Engineering Research Council of Canada (NSERC).

[1] *Sputtering by Particle Bombardment*, edited by R. Behrisch (Springer-Verlag, Berlin, 1983), Vol. II.
[2] *Ion Bombardment Modification of Surfaces*, edited by O. Auciello and R. Kelly (Elsevier, Amsterdam, 1984)
[3] G. Carter, Vacuum **47**, 409 (1996).
[4] Dae Won Moon and Kyung Joong Kim, J. Vac. Sci. Technol. A **14**, 2744 (1996).
[5] S. Rusiponi, G. Costantini, C. Boragno, and U. Valbusa, Phys. Rev. Lett. **81**, 2735 (1998).
[6] J. F. Whitacre, Z. U. Rek, J. C. Bilello, and S. M. Yalisove, J. Appl. Phys. **84**, 1346 (1998).
[7] S. Habenicht, W. Bolse, K. P. Lieb, K. Reinmann, and U. Geyer, Phys. Rev. B **60**, R2200 (1999).
[8] V. K. Smirnov, D. S. Kibalov, and S. A. Krivelevich, Nucl. Instrum. Methods Phys. Res. B **147**, 310 (1999).
[9] F. Frost, D. Hirsch, and A. Schindler, Appl. Surf. Sci. **179**, 8 (2001).
[10] S. Facsko, H. Kurz, and T. Dekorsy, Phys. Rev. B **63**, 165329 (2001).
[11] R. M. Bradley and J. M. E. Harper, J. Vac. Sci. Technol. A **6**, 2390 (1988).
[12] G. Carter, Phys. Rev. B **59**, 1669 (1999).
[13] G. Carter, J. Appl. Phys. **85**, 455 (1999).
[14] M. A. Makeev and A.-L. Barabási, Appl. Phys. Lett. **71**, 2800 (1997).
[15] M. A. Makeev and A.-L. Barabási, Appl. Phys. Lett. **72**, 906 (1998).
[16] M. Makeev and A.-L. Barabási, Appl. Phys. Lett. **73**, 1445 (1998).
[17] S. Park, B. Kahng, H. Jeong, and A.-L. Barabási, Phys. Rev. Lett. **83**, 3486 (1999).
[18] P. Sigmund, Phys. Rev. **184**, 383 (1969).
[19] P. Sigmund, J. Mater. Sci. **73**, 1545 (1973).
[20] M. A. Shaheen and D. N. Ruzic, J. Vac. Sci. Technol. A **11**, 3085 (1993).
[21] M. Küstner, W. Eckstein, V. Dose, and J. Roth, Nucl. Instrum. Methods Phys. Res. B **145**, 320 (1998).
[22] M. Stepanova and S. K. Dew, J. Appl. Phys. **92**, 1699 (2002).
[23] More information from the manufacturer can be found on the web page http://www.selmi.sumy.ua/
[24] V. T. Barchenko, I. S. Balikoev, S. N. Zagranichny, S. V. Pechko, and T. D. Radjabov, Vac. Phys. Technol. **1**, 5 (1993).
[25] I. P. Soshnikov, Yu. A. Kudriavtsev, A. V. Lunev, and N. A. Bert, Nucl. Instrum. Methods Phys. Res. B **127/128**, 115 (1997).